JOURNAL OF MATERIALS SCIENCE 32 (1997) 5355–5362

Transmission electron microscopy of the fibre–matrix interface in SiC–SCS-6-fibre-reinforced IMI834 alloys

H. J. DUDEK, R. BORATH, R. LEUCHT, W. A. KAYSSER
German Aerospace Research Establishment (DLR), Institute of Materials Research, Linder Höha D-51140 Köln, Germany

In SiC–SCS-6-fibre-reinforced IMI834 alloys, a high thermal stability of tensile properties and of the fibre–matrix interface for temperatures up to 700 °C was reported. In the present paper, the interface of these composites is investigated by analytical transmission electron microscopy in the as-processed condition and after a thermal treatment at 700 °C for 2000 h and at 800 °C for 500 h. The interface in (SiC–SCS-6)–IMI834 composites consists of two layers: the TiC reaction zone with a thickness of about 0.4 μm and a layer of a $(Ti, Zr)_xSi_y$ phase with a thickness of about ~0.1 μm. The energy-dispersive electron beam analysis of the $(Ti, Zr)_xSi_y$ layer results in a $(Ti, Zr)_2Si$ phase with a Ti-to-Zr ratio of approximately 1.4. Electron beam diffraction of the $(Ti, Zr)_xSi_y$ layer identifies it as S2 silicides present in near-α alloys. The thermal stability of the interface in the (SiC–SCS-6)–IMI834 composites is ensured by the continuous coating of the $(Ti, Zr)_xSi_y$ phase. This is the case for a thermal treatment at temperatures up to 700 °C for 2000 h. After the treatment at 800 °C for 500 h, the thickness of the TiC reaction zone is increased, gaps in the $(Ti, Zr)_xSi_y$ layer appear, titanium carbide grows further into the titanium matrix and the thermal stability of the interface is lost.

1. Introduction

The thermal stability of the fibre–matrix interface in SiC-fibre-reinforced titanium alloys is one of the most important pre-conditions for the development of composites for high-temperature service applications. In SiC–SCS-6-fibre-reinforced IMI834 (Ti–6 wt% Al–4 wt% Sn–4 wt% Zr–0.70 wt% Nb–0.50 wt% Mo–0.35 wt% Si) alloys the mechanical properties and interface thickness are very stable during thermal treatment [1]. No change in the tensile properties of these composites is observed after a thermal treatment at 700 °C for 2000 h and at 800 °C for 1000 h and the values for tensile strength were in accordance with the predictions of the rule of mixtures. For a fibre volume fraction of 0.35, the tensile strength is 2 GPa, Young's modulus 220 GPa and the elongation at fracture nearly 1.3%. For all annealing times at 700 °C, a constant reaction zone thickness of about 0.5 μm and a constant remaining carbon coating thickness of roughly 3 μm of the SCS-6 fibre were observed. The frictional shear stress between fibre and matrix measured in push-back experiments in these composites was also constant (75 MPa) for all annealing times at 700 °C. In the present investigation, the interfaces in SiC–SCS-6-fibre-reinforced IMI834 alloys in the as-processed condition and after a thermal treatment at 700 °C for 2000 h and at 800 °C for 500 h were investigated by analytical transmission electron microscopy with the aim of understanding the mechanism of the thermal stabilization in these composites.

2. Experimental procedure

SiC–SCS-6-fibre-reinforced IMI834 alloys were processed by fibre coating with matrix and subsequent hot isostatic pressing of bundles of matrix-coated fibres. The fibres were coated with the IMI834 alloy by magnetron sputtering [2, 3]. A slight deviation of the element concentrations for Sn and Al from the nominal concentrations during matrix deposition is observed (nominal concentration of Sn, 4 wt%; measured concentration of Sn, 3 wt%; nominal concentration of Al, 6 wt%; measured concentration of Al, 5.6 wt % [2]). Hot isostatic pressing (HIP) was performed at 190 MPa and 930 °C for 0.5 h. Details of composite processing have been described elsewhere [3, 4]. The oxygen concentration in the matrix after composite processing was 700 wt ppm.

The composites were annealed at 700 °C for up to 2000 h and at 800 °C for up to 1000 h. During heat treatment the hot isostatically pressed samples remained in the stainless steel capsule (used for HIP) to prevent oxidation. After annealing, cylindrical tensile test samples were prepared. The mechanical properties and interface properties have been reported elsewhere [1]. For transmission electron microscopy (TEM), thin slices of a thickness of 500 μm

0022–2461

perpendicular to the fibre axis were cut by a diamond saw and thinned to 200 μm by mechanical polishing. Subsequently, the samples were dimpled with a dimple grinder (Gatan 656) and ion milled using small-angle ion etching with a Gatan PIPS 691. Care was taken to prevent redeposition of matrix material on the TEM specimen during ion milling [5]. The samples were investigated at 300 kV with a Philips EM430 analytical transmission electron microscope attached to a scanning transmission system and a Tracor EDS System 5500. The samples were investigated using a semiquantitative (standardless) energy-dispersive X-ray analysis (EDXA) at an acceptance angle of 70° to the sample normal. No correction for absorption of the X-ray intensities was needed. The EDXA was performed at sufficiently thin sample positions to ensure that only the phase of interest was crossed by the electron beam. Areas not smaller than 30 nm were analysed by an electron beam with a spot size lower than 10 nm. A careful astigmatism correction for the electron beam was performed to ensure that the electron beam was free of a halo. This care is absolutely necessary when the composition of such small regions has to be measured. The spatial resolution of the electron microbeam analysis is documented by the semiquantitative energy-dispersive X-ray line scans. From our experience with the quantitative EDXA analysis in the transmission electron microscope, we consider the relative accuracy to be better than 10% for element concentrations higher than 5 at% (and atomic numbers greater than 11). The phases of interest were investigated by EDXA and electron diffraction in all thermal treatment conditions to ensure that no change in the structure and composition during heat treatment occur.

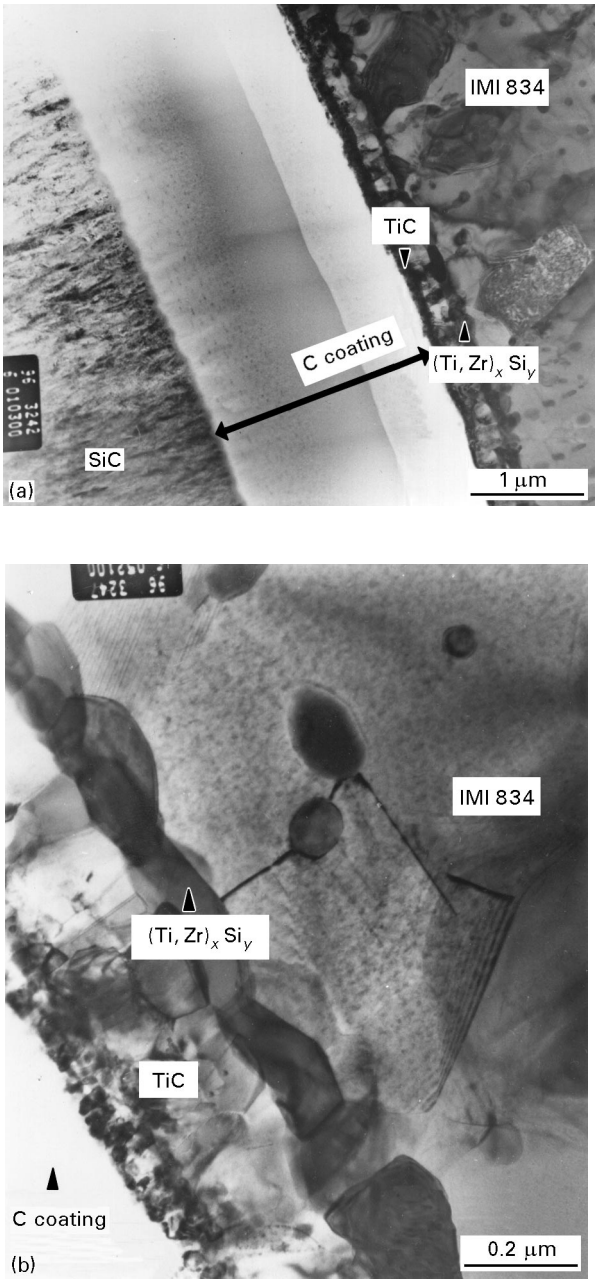

Figure 1 Fibre–matrix interface in as-processed SiC–SCS-6-fibre-reinforced IMI834 alloys: (a) overview for the whole interface; (b) detail of the TiC–$(Ti, Zr)_xSi_y$ -layer.

3. Results

3.1. Interfaces in as-processed composites

In Fig. 1a, an overview of the fibre–matrix interface of the as-processed (SiC–SCS-6)–IMI834 composite is shown. Crossing the image from left to right, the following layers can be identified in Fig 1a. On the left the structure of the SiC fibre is visible. It is followed by the carbon protective coating roughly 3 μm thick of the SiC–SCS-6 fibre. Particles visible in the carbon layer consist of SiC [6, 7]. The variation in the contrast in the carbon coating is due to the variation in the content of the SiC particles. Adjacent to the carbon coating, a fine-grained TiC structure with an approximate thickness of 100 nm is visible which develops into coarser columnar TiC grains (Fig. 1b). The thickness of the fine TiC grain layer varies at different sample positions between 10 and 100 nm. The thickness of the whole TiC layer is nearly constant and roughly 400 nm. (Depending on sample position a scattering of the thickness has to be expected [1].) The TiC layer is completely covered by a layer roughly 30–100 nm thick appearing dark in contrast in the TEM image of Fig. 1. This layer consists of single grains (Fig. 1b). Adjacent to this layer the titanium matrix IMI834 is found. The IMI834 matrix has an α grain size of roughly 1 μm which is typical of our processing method [2, 3]. In some grains of the IMI834 matrix, small particles of a few nanometres appear which are probably α_2 precipitates [8, 9]. In the grains of the matrix and at the grain boundaries, particles of roughly 100 nm size are visible. Such particles were identified in the IMI834 alloy by other workers as S2 silicides [8, 10].

The two TiC layers with a small grain size and large grain size, respectively, are typical of (SiC–SCS-6)–titanium matrix composites in the as-processed condition. This structure of the interface was also observed for example in (SiC–SCS-6)–(Ti–6 wt% Al–4 wt% V) [5, 11], in (SiC–SCS-6)–Ti–1421 and in (SiC–SCS-6)–Ti-6242 [12] composites. The layer appearing dark in contrast which separates the TiC layers from the titanium matrix is unusual. This layer was investigated in detail by semiquantitative EDXA, semiquantitative

TABLE I Semiquantitative energy-dispersive X-ray results of the $(Ti, Zr)_xSi_y$ phase and of particles in the matrix of (SiC–SCS-6)–IMI834 composites for different thermal treatment conditions where N is the number of point analyses

Composite condition	Concentration (at %) obtained by semiquantitative energy-dispersive X-ray chemical analysis							N
	Ti	Zr	Si	Al	Sn	Nb	Mo	
As-processed $(Ti, Zr)_xSi_y$	40.5 ± 2.1	25.0 ± 1.3	31.6 ± 1.1	2.1 ± 0.5	0.4 ± 0.2	0.3 ± 0.1	0.0	10
As processed S2 particles	38.2 ± 2.3	27.6 ± 1.2	30.6 ± 1.8	2.4 ± 0.8	0.8 ± 0.4	0.3 ± 0.2	0.0	10
$(Ti, Zr)_xSi_y$ (700 °C for 2000 h)	39.6 ± 2.4	25.1 ± 2.5	31.8 ± 2.5	1.9 ± 0.8	0.7 ± 0.7	0.4 ± 0.2	0.0	11
S2 particles (700 °C for 2000 h)	38.9 ± 1.8	27.6 ± 2.2	30.4 ± 2.1	1.5 ± 1.1	0.7 ± 0.3	0.3 ± 0.2	0.0	11
$(Ti, Zr)_xSi_y$ (800 °C for 500 h)	37.7 ± 3.2	27.4 ± 3.1	31.8 ± 1.2	2.1 ± 0.9	0.6 ± 0.3	0.4 ± 0.2	0.0	19
S2 particles (800 °C for 500 h)	37.2 ± 1.2	28.5 ± 2.0	30.3 ± 1.5	2.2 ± 1.1	0.9 ± 0.3	0.3 ± 0.3	0.0	15

energy-dispersive X-ray line scans and electron diffraction. In Table I, results of semiquantitative EDXA of this layer are summarized for different thermal treatment conditions and compared with the chemical element concentration of the roughly 100 nm large particles found in the IMI834 matrix.

In Fig. 1b the layer is shown at a higher magnification, and in Fig. 2 and Fig. 3 electron diffraction patterns of the crystals of the layer between the TiC reaction zone and IMI834 matrix, and of the S2 particles in the IMI834 matrix, respectively, are shown for the three sample conditions. (For every case and sample condition, diffraction patterns for three different orientations were determined; in the paper only one is reproduced. Our aim was to ensure that during thermal treatment in the particles and in the layer no chemical and structural changes occur.) The electron diffraction patterns of the layer (Fig. 2a), and the particles in the matrix (Fig. 3a) can be indexed by the assumption that they consist of hexagonal S2 silicides [13–15] with the lattice constants $a = 0.699\,35$ nm, $c = 0.367\,63$ nm and $c/a = 0.526$ [14]. (The diffraction patterns contain mostly high-index zones because the silicide crystals are differently oriented in the interface and in the matrix.) For convenience in this paper, the layer between the TiC reaction zone and the IMI834 matrix will be called the $(Ti, Zr)_xSi_y$ phase.

In Fig. 4, a typical semiquantitative energy-dispersive X-ray line scan across the $(Ti, Zr)_xSi_y$ phase of an as-processed composite is shown. From the energy-dispersive X-ray line scan, a spatial resolution of approximately 10 nm results. The measured $(Ti, Zr)_xSi_y$ phase has at this interface position a thickness of roughly 30 nm. In Table I, the mean values and the standard deviation of the concentration of the elements in the $(Ti, Zr)_xSi_y$ phase and in the S2 particles of the IMI834 matrix are given. The measurements were performed at ten or more different positions of the S2 particles and of the $(Ti, Zr)_xSi_y$ phase. The mean concentrations of the elements Ti, Zr and Si in the S2 silicides are nearly 38.2 at%, 27.6 at% and 30.6 at%, respectively. In the $(Ti, Zr)_xSi_y$ phase of the as-processed sample, the concentrations of the elements Ti, Zr and Si are the same as those of the S2 silicides when the scattering range of the analysis results is considered. The mean values are 40.5 at% for Ti, 25.0 at% for Zr and 31.6 at% for Si. The relative standard deviation is of the order of 5% and in the range of the relative accuracy of this analysis method. The structure and chemical composition of the $(Ti, Zr)_xSi_y$ phase and the S2 silicide particle in the matrix are the same; the $(Ti, Zr)_xSi_y$ phase consists of S2 silicides.

3.2. Interface in composites treated at 700 °C for 2000 h

In Fig. 5 the interface region of (SiC–SCS-6)–IMI834 composites thermally treated at 700 °C for 2000 h is shown. No significant difference between the thermally treated condition and the as-processed condition (Fig. 1) can be observed. Again the interface consists of two layers: of the TiC reaction zone and of the $(Ti, Zr)_xSi_y$ layer with thicknesses of roughly 0.4 μm, respectively. The thicknesses of both layers remain nearly unchanged during the thermal treatment at 700 °C for 2000 h. (A statistical variation in the thickness for the same treatment conditions is observed owing to the technical conditions of sample processing; the stability of the reaction zone and carbon layer thickness during thermal treatment was shown in [1].) As can be concluded from the semiquantitative analysis data (Table I), the concentrations of elements in the $(Ti, Zr)_xSi_y$ phase for that treatment condition are roughly the same as in the as processed sample when the standard deviation of the results is considered. From the line scan (Fig. 6), a resolution of about 10 nm is deduced and the thickness of the $(Ti, Zr)_xSi_y$ phase at this interface position is of the order of 55 nm. Element concentrations in the $(Ti, Zr)_xSi_y$ phase of 39.6 at% for Ti, 25.1 at% for Zr and 31.8 at% for Si are now measured. During treatment at 700 °C for 2000 h, the concentrations of the elements Ti, Zr and Si in the S2 silicides have not changed either and are 38.9 at%, 27.6 at% and 30.4 at%, respectively. Electron diffraction patterns of the particles in the matrix

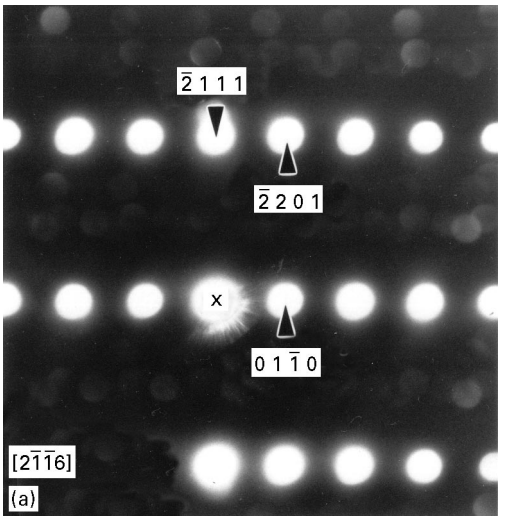

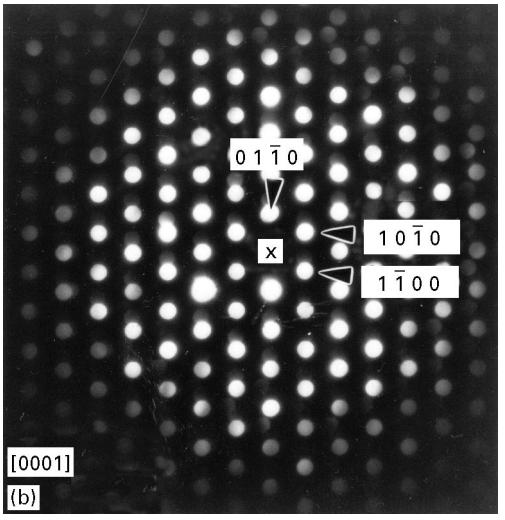

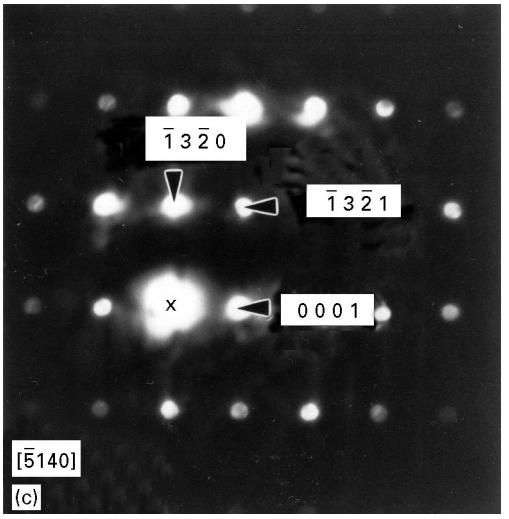

Figure 2 Electron diffraction diagrams of the $(Ti, Zr)_xSi_y$ phase for the three different sample conditions, namely (a) as processed, (b) 700 °C for 2000 h and (c) 800 °C for 500 h, identifying them as S2 silicides.

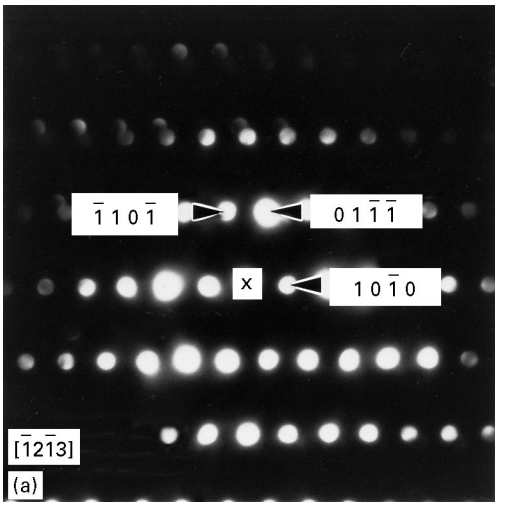

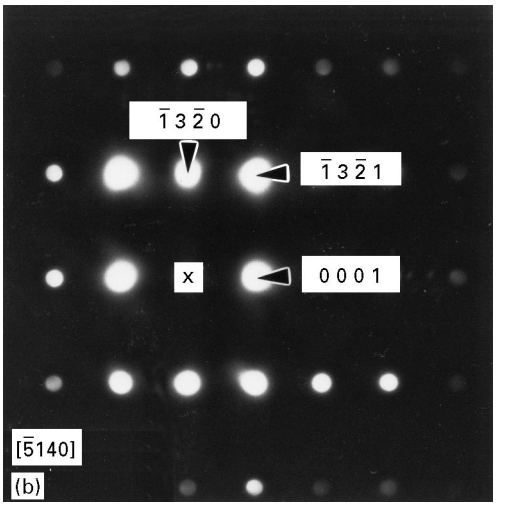

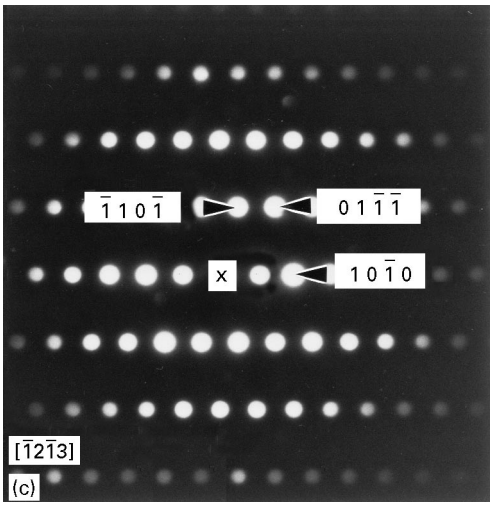

Figure 3 Electron diffraction diagrams of the particles in the IMI834 alloy for the three different sample conditions, namely (a) as processed, (b) 700 °C for 2000 h and (c) 800 °C for 500 h, identifying them as S2 silicides

and the $(Ti, Zr)_xSi_y$ phase result again in the hexagonal S2 silicide structure (Fig 2b and Fig. 3b).

3.3. Interface in composites treated at 800 °C for 500 h

In Fig. 7, the interface region for (SiC–SCS-6)–IMI834 composites treated at 800 °C for 500 h is shown. Compared with the as-processed samples and with those samples treated at 700 °C for 2000 h, the composite treated at 800 °C for 500 h still has unchanged tensile properties, as was reported in [1]. At first sight, the same interface as in the as-processed condition is observed. The semiquantitative analysis of the $(Ti, Zr)_xSi_y$ phase and of the S2 silicides in the

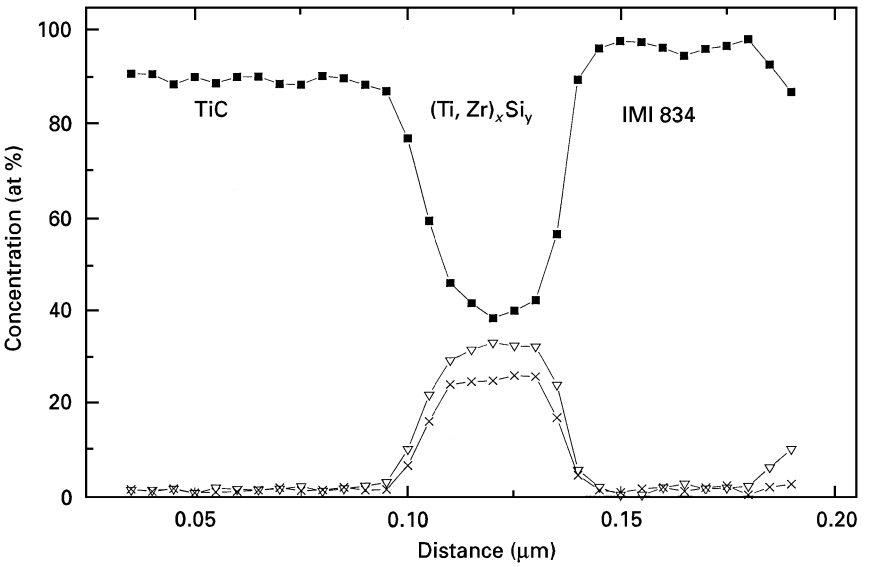

Figure 4 Semiquantitative energy-dispersive X-ray line scan across the TiC–(Ti, Zr)$_x$Si$_y$ layer in the as-processed composites. (■), Ti; (▽), Si; (×), Zr.

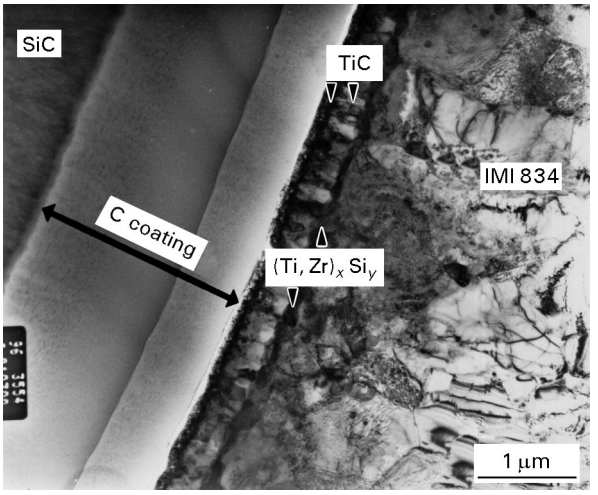

Figure 5 Fibre–matrix interface in SiC–SCS-6-fibre-reinforced IMI834 alloys thermally treated at 700 °C for 2000 h.

IMI834 alloy shows nearly the same composition as in the as-processed samples. A slight increase in zirconium (and decrease in titanium) in the (Ti, Zr)$_x$Si$_y$ phase (Table I) from the mean value of 25 at% for the as-processed condition to 27.5 at% in samples treated at 800 °C for 500 h is observed. This change in the element concentration is probably not real, because it is still inside the region of standard deviation of our analysis results. Again, the hexagonal S2 phase both in the (Ti, Zr)$_x$Si$_y$ phase and in the particles is identified by electron diffraction (Fig. 2c and Fig. 3c).

A detailed investigation of the interface in this composite shows many differences in comparison with the other two investigated composites, however. The thickness of the carbon protective coating of the SiC–SCS-6 fibre is now reduced to a value of roughly 2.4 μm and the thickness of the whole TiC reaction zone is increased to roughly 2.1 μm. The (Ti, Zr)$_x$Si$_y$

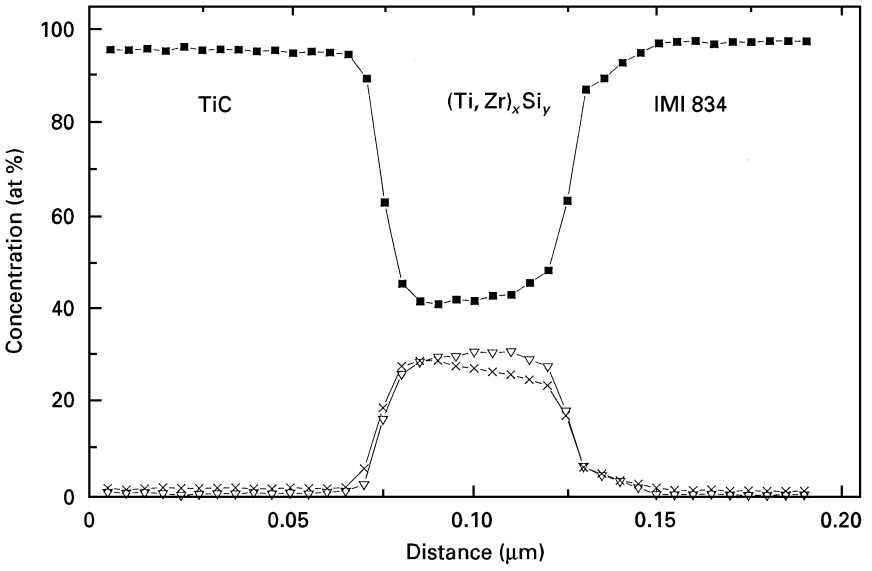

Figure 6 Semiquantitative energy-dispersive X-ray line scan across the TiC–(Ti, Zr)$_x$Si$_y$ layer of the composite treated at 700 °C for 2000 h. (■), Ti; (▽), Si; (×), Zr.

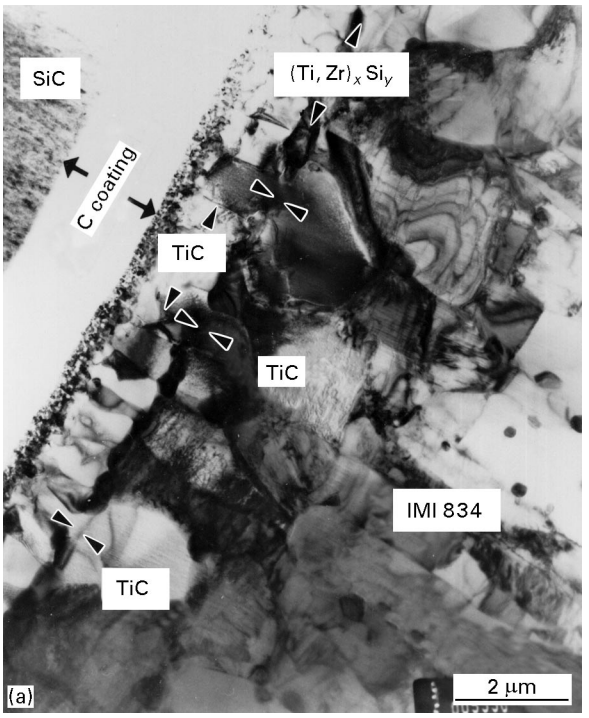

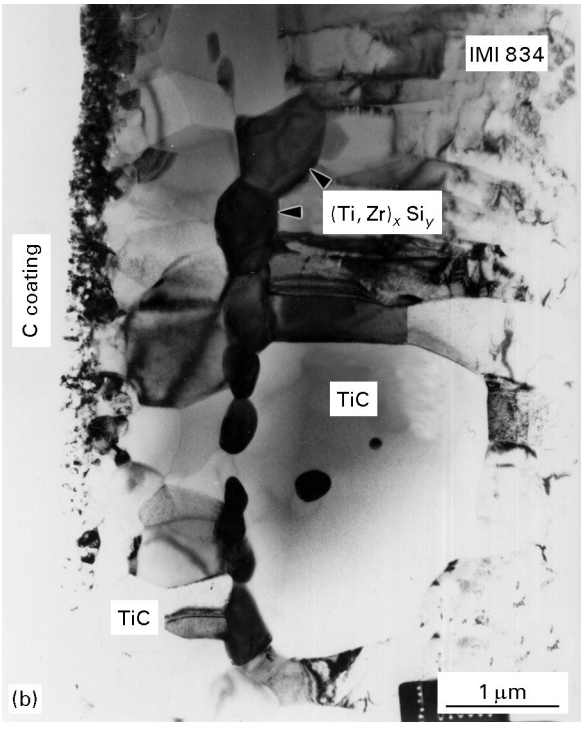

Figure 7 Fibre–matrix interface in SiC–SCS-6-fibre-reinforced IMI834 alloys thermally treated at 800 °C for 500 h: (a) overview; (b) detail of the TiC–(Ti, Zr)$_x$Si$_y$ layer.

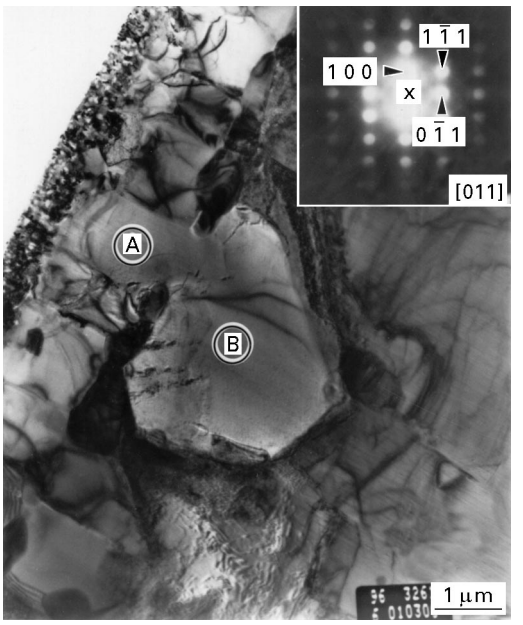

Figure 8 TiC grain growing from the previous reaction zone between the carbon coating and the (Ti, Zr)$_x$Si$_y$ layer into matrix and electron diffraction diagram from positions A and B showing that this grain is one single TiC crystal.

layer now does not completely cover the TiC layer. In Fig. 7b a detail of the interface is shown at a higher magnification. At this position a gap is found in the (Ti, Zr)$_x$Si$_y$ phase and the TiC grain has grown from the TiC reaction layer into the inside of the IMI834 matrix. Such a position is investigated in Fig. 8. Diffraction patterns were measured at the position A and B in Fig. 8, i.e., on both sides of the (Ti, Zr)$_x$Si$_y$-layer. The diffraction patterns show at both positions the same orientation of the TiC grain. During thermal treatment the TiC grain has grown from the TiC layer of the previous reaction zone into the titanium matrix passing through the gap of the (Ti, Zr)$_x$Si$_y$ layer. In Fig. 7b an S2 particle probably having covered the gap now is inside the TiC particle. Similar effects were found at many positions of the interface. They are indicated in Fig. 7a by arrowheads.

4. Discussion

4.1. Formation of the S2 silicide and the (Ti, Zr)$_x$Si$_y$ phase

The matrix material in our composites has a different history in comparison with the IMI834 alloy described in the literature (see, for example, [8, 10]). In our case, the matrix is deposited on the fibres by magnetron sputtering. The deposition temperature is roughly 500 °C. The grain size in the as-deposited material is of the order of 100 nm. It can be assumed that the deposition procedure favours a fine disperse distribution of the alloying elements in the matrix which will be similar to a solution heat treatment at temperatures above the β transus (the β transus temperature for the IMI834 alloy is 1045 °C). After HIP a grain size of 0.5–1.0 μm is usually observed in the IMI834 matrix [4]. During HIP at 930 °C for 0.5 h, no silicide formation will probably take place. This can be concluded from the following considerations. The first formation of silicides in a similar alloy IMI829 (Ti–5.4 wt% Al–3.5 wt% Sn–3 wt% Zr–1 wt% Nb–0.3 wt% Mo–0.3 wt% Si) during cooling from a temperature above the β transus is observed after 930 °C for 1.4 h [16]. The cooling rate after composite processing in our hot isostatic press is of the order of 0.5 °C s^{-1} between 930 and 600 °C and of the order of 0.1 °C s^{-1} between 600 and room temperature [17]. In the IMI829 alloy, the S2 silicide precipitation occurs during cooling from the solution heat treatment

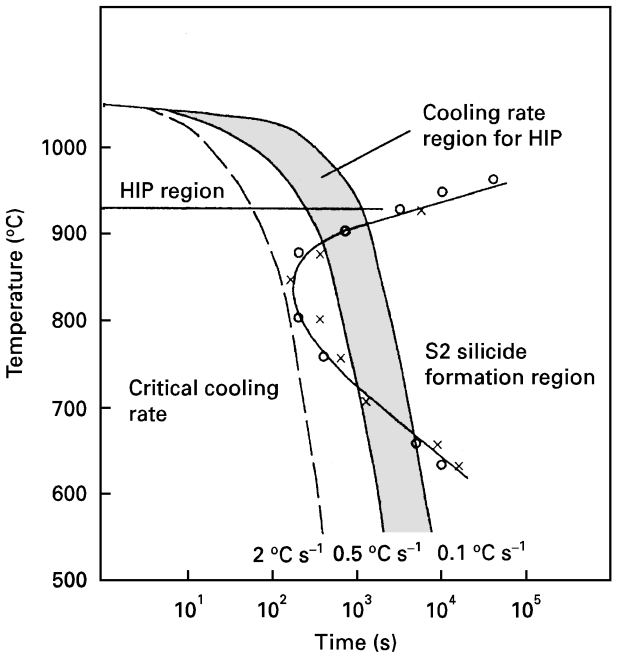

Figure 9 Time–temperature-precipitation curve for the S2 silicide formation according to [16] for the illustration of the formation of the (Ti, Zr)$_x$Si$_y$ phase at the TiC reaction zone during cooling after HIP. (○), no silicides observed; (×), silicides first observed. The region of S2 silicide formation was determined in [16] for the IMI829 alloy.

temperature for cooling rates lower than 2 °C s^{-1} [16]. From this we conclude that the observed S2 silicides in our samples in the as-processed condition are forming during cooling after HIP. The structure of the interface is another hint that most of the silicide formation takes place during cooling; the (Ti, Zr)$_x$Si$_y$ crystals form in the interface between the TiC reaction zone and the IMI834 alloy, which can only be the case when the carbon–titanium reaction is completed. When the silicide formation takes place during the time of HIP at 930 °C (this is the period in which the TiC reaction zone formation occurs) then we observe S2 particles mostly inside the TiC layer and not at the TiC–matrix interface. The S2 silicide formation during our processing conditions is illustrated in Fig. 9.

4.2. Mechanism of interface formation

For the formation of the fibre–matrix interface in our composites the following mechanism is proposed. During composite processing at 930 °C for 0.5 h, the carbon protective coating of the SCS-6 fibre reacts with the titanium alloy to form TiC. This reaction is similar to that observed in other composites [5, 11, 12]. As small amounts of silicon are present in the carbon coating of the SiC–SCS-6 fibre, they will form titanium silicides at the same time. TiC is predominantly formed in direct contact to the surface of the carbon coating of the fibre and silicides form mostly outside the TiC layer [18]. The formation of silicides from the silicon in the carbon coating may favour the segregation of the (Ti, Zr)$_x$Si$_y$ phase observed in the interface of our as-processed composites. The silicon of the IMI834 alloy, being finely dispersed in the matrix owing to the matrix deposition procedure on the fibres, will segregate together with zirconium to the fibre–matrix interface during cooling to form the observed (Ti, Zr)$_x$Si$_y$ layer. From the homogeneous (Ti, Zr)$_x$Si$_y$ coating completely covering the TiC layer we conclude that the wettability of the TiC by silicides is larger than that for the titanium alloy. The same element concentration in the (Ti, Zr)$_x$Si$_y$ phase and the same crystallographic structure as in the S2 silicide shows that a similar segregation mechanism is in action for both cases.

4.3. Composition of the S2 silicide and the (Ti, Zr)$_x$Si$_y$ phase

After processing, the element concentrations of Zr and Si seem to be nearly in equilibrium in the S2 silicide particles. Most of the free silicon previously present in the matrix is bonded in the S2 silicides and in the (Ti, Zr)$_x$Si$_y$ phase. This follows from the observation that no significant change in the element concentration nor in the structure determined by electron diffraction in the S2 silicides is observed even after treatment at 800 °C for 500 h. The structure of the particles and the (Ti, Zr)$_x$Si$_y$ phase is that of the S2 silicides and the element concentration is roughly $Ti_{38}Zr_{27.5}Si_{31.5}$, which identifies them as a (Ti, Zr)$_2$Si compound with a Ti-to-Zr ratio of 1.38. The Ti-to-Zr ratio is in the range between 2.26 and 0.68 which was reported previously [14]. 2 at% Al and small amounts of Sn (about 0.5 at%) were also found in the S2 silicides and in the (Ti, Zr)$_x$Si$_y$ phase. A substitution of Si by small amounts of Al [19] and Sn [20] in silicides was reported in the literature. No molybdenum was found in either phase.

No significant change in the concentrations of the elements Zr and Si results when annealing the composites at 700 °C for 2000 h. The mobilities of the silicon and zirconium bonded in silicides are low at these conditions. A similar high stability of the reaction zone thickness at temperature of 650 °C was also found in Ti–6 wt% Al–2 wt% Sn–4 wt% Zr–2 wt% Mo alloy and silicides of the composition (Ti, Zr)$_5$Si$_3$ were identified in the interface by Ritter *et al.* [12]. From the present work we conclude that the high interface stability observed in composites in [12] should also be attributed to the silicide layer probably present in these composites.

4.4. Loss of interface stability during heating

According to McIntosh and Baker [16], the S2 silicides should still remain stable for temperatures higher than 700 °C. In a similar alloy, IMI829, no solution of the S2 silicides is observed for temperatures up to 970 °C. We expect, therefore, that at 800 °C the observed instability of the fibre–matrix interface leading to a growth of the TiC reaction zone and the growth of TiC grains behind the (Ti, Zr)$_x$Si$_y$ barrier (Fig. 7b and Fig. 8) is not caused by dissolution of the (Ti, Zr)$_x$Si$_y$ phase. In fact, in the neighbourhood of the TiC grain growing into the matrix, silicides are found (Fig. 7b) which were probably located at the interface to the

TiC layer in the as-processed condition. The reaction between titanium and carbon at the interface in the samples treated at 800 °C for 500 h is driven by the increased diffusion of titanium and carbon at grain boundaries of the $(Ti, Zr)_xSi_y$ phase at this temperature. The growth of the TiC reaction zone and the growth of TiC grains behind the $(Ti, Zr)_xSi_y$ phase into the IMI834 matrix is accompanied by a change in the particle geometry [16]. This assumption is supported by the observation of particle shape variation in the IMI834 alloy at 700 °C described in [10, 21].

5. Conclusions

The formation of the $(Ti, Zr)_xSi_y$ phase at the interface of (SiC–SCS-6)–IMI834 composites during processing explains the observed high thermal stability of tensile and interface properties of these composites during post-processing thermal treatment [1]. The stabilization is governed by the $(Ti, Zr)_xSi_y$ phase which prevents progress of the reaction between the titanium alloy and the carbon coating during heat treatment. A thickness of only one grain size with a diameter of less than 100 nm is sufficient to prevent a progress of the interaction for thermal treatments at temperatures up to 700 °C for 2000 h. The nearly unchanged thickness of the TiC reaction zone after the treatment at 700 °C for 2000 h shows that the $(Ti, Zr)_xSi_y$ layer is an effective diffusion barrier for titanium and carbon.

At higher temperatures, e.g., at 800 °C , enhanced titanium and carbon diffusion at grain boundaries and the reorganization of the shape of the $(Ti, Zr)_xSi_y$ phase initiate the reaction between the carbon coating and the titanium matrix and the interface stabilization effect of the $(Ti, Zr)_xSi_y$ phase is gradually lost. After a thermal treatment at 800 °C for treatment times of 500 h the stabilization effect disappears and for treatment times higher than 1000 h the tensile properties of the composites are lowered to values of the unreinforced matrix material [1].

From the present results, one can expect that the formation of the $(Ti, Zr)_xSi_y$ phase at the fibre–matrix interface will take place in all near-α alloys with similar concentrations of the elements Zr and Si and processed by fibre coating with matrix applied in this work. A formation of a closed $(Ti, Zr)_xSi_y$ layer on the fibre can preferentially be expected when the elements Zr and Si are dissolved in the matrix and not bonded in silicides.

The processing line of the titanium matrix composites is of exceptional importance for the stability of the fibre–matrix interface during thermal treatment. In the case of SiC–IMI834 composites the formation of the silicide layer will probably not take place when HIP is performed below 930 °C or when the HIP time is much longer than 1 h (Fig. 9). For temperatures below 930 °C and long HIP times the S2 silicides will partly segregate during consolidation inside the TiC reaction zone and will probably not form a continuous layer separating the TiC zone from the matrix.

It should be possible to realize a similar self-stabilization effect of the interface also in quite different composite systems. Pre-conditions for this effect are the solution of alloying elements in the matrix at processing temperatures, segregation of these elements in phases during cooling after processing and higher wettability of the fibre surface by the precipitating phase in comparison with the matrix material. In addition, the phases segregating to the interface have to be stable at service temperatures and they should be a diffusion barrier for the reacting elements of the matrix and the fibre.

References

1. H. J. DUDEK, R. LEUCHT and J. HEMPTENMACHER, *Metall. Trans. A* **27** (1996) 1403.
2. R. LEUCHT, H. J. DUDEK, K. WEBER and A. WERNER, *Z. Metallkde* **87** (1996) 424.
3. R. LEUCHT and H. J. DUDEK, *Mater. Sci. Engng A* **188** (1994) 201.
4. H. J. DUDEK, R. LEUCHT and W. A. KAYSSER, in Proceedings of the Tenth International Conference on Composite Materials, Whistler, BC, August 1995, Vol. II, (Wood head, Vancouver, 1995) pp. 695–702.
5. H. J. DUDEK, R. LEUCHT, R. BORATH and G. ZIEGLER, *Mikrochim. Acta.* (*Wein*) *Suppl.* II (1990) 137.
6. X. J. NING and P. PIROUZ, *J. Mater. Res.* **6** (1991) 2234.
7. M. LANCIN, J. THIBAULT-DESSEAUX and J. S. BOUR, *J. Microsc. Spectrosc. Electron.* **13** (1988) 503.
8. C. REMACHANDRA, A. K. SINGH and G. M. K. SARA, *Metall. Trans. A* **24** (1993) 1273.
9. G. SRIDHAR and D. S. SARMA, *ibid.* **19** (1988) 3025.
10. P. GHOSAL, R. PRASAD and C. RAMACHANDRA, *ibid.* **26** (1995) 2751.
11. C. G. RHODES and R. A. SPURLING, in "Recent advances in composites in the United States and Japan", ASTM Special Technical Publication 864, edited by J. R. Vinson and M. Taya (American Society for Testing and Materials, Philadelphia, PA, 1983), pp. 585–99.
12. A. M. RITTER, E. L. HALL and N. LEWIS, *Mater. Res. Soc. Symp. Proc.* **197** (1990) 413.
13. H. M. FLOWER, P. R. SWANN and D. R. F. WEST, *Metall. Trans.* **2** (1971) 3289.
14. N. H. SALPADORU and H. M. FLOWER, *Metall. Trans. A* **26** (1995) 243.
15. A. P. WOODFIELD and M. H. LORETTO, *Scripta Metall.* **21** (1987) 229.
16. G. McINTOSH and T. N. BAKER, in Proceedings of the Sixth World Conference on Titanium, Vol. III, edited by P. Lacombe, R. Tricot and G. Beranger (Society Francaise Metallurgie, 1988) pp. 1571–76.
17. R. LEUCHT, K. WEBER, H. J. DUDEK and W. A. KAYSSER, in Proceedings of the Seventh European Conference on Composite Materials, (ECCM-7) vol. 1, 14–16 May 1996, Institute of Materials, London (Wood head, Cambridge, 1996) pp. 361–66.
18. H. J. DUDEK, L. A. LARSON and R. BROWNING, *Surf. Interface Anal.* **6** (1984) 274.
19. Z. ZHANG and H. M. F. FLOWER, *Mater. Sci. Technol.* **7** (1991) 812.
20. G. McINTOSH and T. N. BAKER, in "Phase transformations—1987" edited by G. W. Lorimer (Institute of Metals, Brookfield, VT, 1988) pp. 115–18.
21. G. SRIDHAR and D. S. SARMA, *Metall. Trans. A* **20** (1989) 55.

Received 9 October 1996
and accepted 1 May 1997